Plasmon Resonances of Graphene-Assisted Core-Bishell Nanoparticles

Hesham Fares (hesham.fares@lnf.infn.it)
Assiut University
Moustafa Ahmed
Minia University
Samar Moustafa
Assiut University

Research Article

Keywords: Core–bishell nanoparticle, Graphene plasmons, Surface plasmon resonance, Plasmonic sensing, Photothermal therapy

Posted Date: May 26th, 2022

DOI: https://doi.org/10.21203/rs.3.rs-1660484/v1

Plasmon Resonances of Graphene-Assisted Core-Bishell Nanoparticles

Hesham Fares[1,2,*] · Moustafa Ahmed[3] · Samar Moustafa[1,2]

[1]*Department of Physics, Faculty of Science, Assiut University, Assiut 71516, Egypt*

[2]*Physics Department, Faculty of Science, Taibah University, P. O. Box 30002, Medina, Saudi Arabia*

[3]*Department of Physics, Faculty of Science, Minia University, 61519 Minia, Egypt*

E-mail address: hesham.fares@lnf.infn.it Tel: +966565718694

Abstract

We study the Localized Surface Plasmon Resonance (LSPR) in graphene-assisted core-bishell nanoparticles which consists of a graphene layer (outer shell) wrapped around a metal shell and either a dielectric or metal core. Small nanoparticles with a size much smaller than the wavelength of incident light are assumed, and the quasi-static approximation is applied to develop analytic equations to describe the absorption, scattering, extinction efficiencies in the core-bishell nanoparticles. The proposed nanostructures exhibit two LSPRs; one is in the visible range and corresponds to a plasmon mode of the core-inner shell composite while the second lies in the near infrared and is induced by the graphene plasmons excited at the outer shell. Interestingly, the latter LSPR of graphene has an ultra-narrow bandwidth and can be tuned in the NIR by altering the physical parameters of graphene, such as the Fermi energy and the number of graphene layers. Therefore, the LSPR peak of graphene is promising for medical applications. In addition, the LSPR of graphene can be tuned to the visible range near the position of the first LSPR, resulting in two narrow linewidth peaks. These resonance peaks could be beneficial for high-sensitive LSPR-based sensors.

Keywords Core–bishell nanoparticle · Graphene plasmons · Surface plasmon resonance · Plasmonic sensing · Photothermal therapy

Introduction

Localized Surface Plasmon Resonance (LSPR) refers to a resonant collective oscillation of conduction electrons on a nanomaterial surface illuminated by light with a frequency similar to that of free electron oscillations. LSPRs in metal nanoparticles result in a localized electromagnetic (EM) field that is associated with light scattering and absorption. Metal nanoparticles have found widespread use in biosensing, imaging, and medical applications [1-10]; thanks to the LSPR's optical properties. Core-shell nanoparticles have conventionally been used to improve the optical properties of LSPRs. Massive efforts have been devoted to core-shell nanoparticles consisting of gold/silver as plasmonic material, sometimes in combination with other materials such as semiconductors and magnetic materials [11]. The LSPR properties of gold/silver-related nanostructures can be tailored by varying the particles size or using different shapes like nanorods [12], nanostars [13,14], nanorice [15], and nanocages [16]. Also, LSPRs of the nanoshell can be tuned by varying the metallic shell thickness scaled by the particle size [17,18].

Graphene is the thinnest material known (i.e., one-atom-thick material), so graphene plasmons exhibit exceptionally light localization. The interest in graphene as a plasmonic material is attributed to the ability to tune its plasmon resonance by adjusting the Fermi level through electrostatic gating, chemical doping, and optical excitation [19]. In addition to the unique characteristics of graphene, such as high intrinsic carrier mobility [20] and broad absorption spectrum of light [21], its excellent light-to-current conversion with internal quantum efficiency close to 100% [22] has made it a promising candidate for advanced optoelectronic devices [23-26]. However, for further implementation of graphene in modern applications, such as tunable modulator, photodetectors, and solar cells [22-27], the relatively low light absorption ($\sim 2.3\,\%$) must be enhanced [21,28]. An effective way to improve the optical absorption is to induce LSPRs absorption in graphene. However, the wavelength of plasmonic resonance in graphene is typically in the mid-infrared range with limited tunability [29]. Light could be concentrated into wavelength volumes leading to enhancements in LSPRs by coating the nanoparticle surface with a graphene layer [30]. The use of metal-graphene and dielectric-graphene hybrids in nanoparticle structures have been theoretically predicted and experimentally demonstrated as an efficient way to enhance the Vis-NIR light absorption in graphene, including core with single-shell [26,29-43] and double-shell [44-48]. The feasibility of fabricating core-shell nanoparticles with graphene shell were demonstrated in many studies [49-53].

High scattering efficiency and an extremely narrow linewidth of plasmonic resonance in the visible range are necessary for LSP-based sensing and imaging applications. LSPRs with strong absorption and narrow line width in the NIF (biological transparent windows of 700-900 nm and 1000-1700 nm) are essential for effective photothermal therapy [54-58]. In order to enhance the spectral properties of LSPRs, graphene shell wrapped around a dielectric core, core–shell nanoparticle, and even with multiple nanoshells [11,17,26,29-53] have been proposed. Fares et al. [43] applied the quasi-static approach to model graphene wrapped around a low−loss dielectric core predicting enhancement of the spectral properties of LSPRs. It was shown that the graphene nanoshell can support two LSPRs with resonance modes corresponding to the symmetric and antisymmetric dipole-like modes in the hybridization theory. The observed resonance modes were characterized by narrow bandwidth and a broadband resonance tunable in the Vis-NIR range [53].

In the present work, we investigate the LSPRs of core-bishell nanoparticles illuminated by incident light. The proposed nanoparticles consist of dielectric core, inner shell of gold/or/silver, and outer shell of graphene. We show significant improvements to the LSPR of conventional metal shell/dielectric core nanoparticles by coating it with a graphene layer. The situation of using a metallic core is also examined in order to compare the absorption efficiency to that of a dielectric core. The present study is restricted to nanoparticles with a small size compared to the wavelength of incident light (i.e., the particle radius $\leq$ 50 nm). Therefore, we exploit the quasi-static formulation to describe the fundamental cross-sections (i.e., scattering, absorption, and extinction) of core-bishell nanoparticles. We show that when using graphene as an outer shell, two separate LSPR peaks can be exhibited in the visible and NIF range. One resonance peak is in the visible range and corresponds to the inner shell wrapped around the core (typical core-shell nanoparticle), while the second peak lies in the NIR range and corresponds to the plasmons of the graphene outer shell. The second LSPR peak of graphene shell is extremely narrow and can be employed in medicinal applications. By varying the optical properties of graphene, such as the Fermi energy and number of graphene layers, we show that the resonance peak controlled by the graphene shell can be tuned to a position nearby the first resonance peak. This leads to a significant linewidth narrowing of the first visible resonance peak, which could be beneficial for high-sensitive LSPR-based sensors.

Methodology

The geometry of the core–bishell nanostructure is schematically shown in Fig. 1 The composite nanoparticle consists of core, inner shell, graphene outer shell, and surrounding medium with primitivities of ϵ_1, ϵ_2, ϵ_3, and ϵ_4, respectively. The core has a radius of r_1, the thickness of the first shell is d, and the thickness of the wrapping graphene shell is t_g.

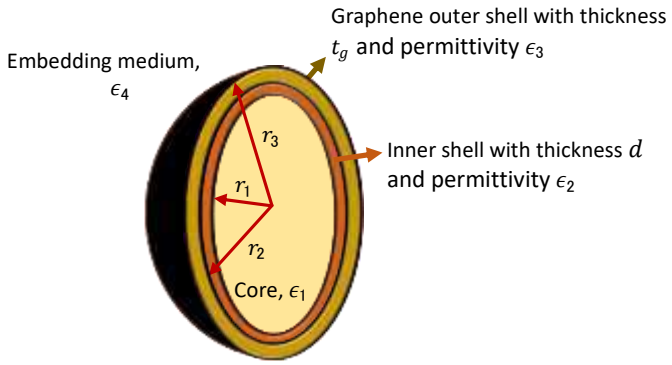

Fig. 1 Schematic of a core bi-shell nanostructure with graphene shell of thickness t_g is wrapping on a dielectric core-shell. The designed nanocomposite embedded in a non-absorbing dielectric medium.

In the quasi-static approach, the dipole electric field $\boldsymbol{E}$ is obtained by solving the Laplace's equation $\nabla^2\Phi = 0$ for the potential Φ along with applying the boundary conditions. In the spherical coordinate system, the solution of the Laplace's equation in each region is given by [58]

$$\Phi_i = \left[A_i r + \left(\frac{B_i}{r^2}\right)\right]\cos(\theta), \tag{1}$$

where $\boldsymbol{E}_i = -\boldsymbol{\nabla}\Phi_i$. The subscript i is the region index, $i = 1,2,3,4$ refers to the core, first shell, second shell, and host medium, respectively.

The following boundary conditions must be met at each interface separating two successive media in Fig. 1 [58],

$$\left.\frac{\partial\Phi_i}{\partial\theta}\right|_{r=r_i} = \left.\frac{\partial\Phi_{i+1}}{\partial\theta}\right|_{r=r_i}, \tag{2-a}$$

$$\epsilon_i\left.\frac{\partial\Phi_i}{\partial r}\right|_{r=r_i} = \epsilon_{i+1}\left.\frac{\partial\Phi_{i+1}}{\partial r}\right|_{r=r_i}. \tag{2-b}$$

With the help of (Eq.1), (Eq. 2) become

$$A_i r_i + \frac{B_i}{r_i^2} = A_{i+1} r_i + \frac{B_{i+1}}{r_i^2}, \tag{3}$$

$$\epsilon_i\left(A_i - 2\frac{B_i}{r_i^3}\right) = \epsilon_{i+1}\left(A_{i+1} - 2\frac{B_{i+1}}{r_i^3}\right), \tag{4}$$

respectively. In the core region (region 1) where r varies from 0 to r_1, $B_1 = 0$. In the embedding medium (region 4) where r varies from r_3 to ∞, $A_4 = -E_0$, and then we recover the potential $\Phi_4 =$

$-E_0 r\cos(\theta)$ far from the second shell. Using (Eq.1) and then applying (Eqs. 3 and 4) at the structure interfaces [**see the supplementary material**], one obtains the electric field at each region in the form of

$$\boldsymbol{E}_i = \left[2\left(\frac{B_i}{r^3}\right) - A_i\right]\cos(\theta)\,\hat{\boldsymbol{r}} + \left[\left(\frac{B_i}{r^3}\right) + A_i\right]\sin(\theta)\,\widehat{\boldsymbol{\theta}}, \tag{5}$$

where

$$A_1 = A_4\left[\frac{A_2}{A_4} + \frac{B_2}{A_4}\frac{1}{r_1^3}\right], \qquad B_1 = 0,$$

$$A_2 = A_4\left[\frac{B_2}{A_4}\frac{C_4}{r_2^3 C_3} - \frac{C_5}{C_3}\right], \qquad B_2 = A_4\frac{(\epsilon_1 - \epsilon_2)}{\left[(\epsilon_1 + 2\epsilon_2) + (\epsilon_1 - \epsilon_2)\left(\frac{C_4}{C_3}\frac{r_1^3}{r_2^3}\right)\right]}\left(\frac{C_5}{C_3}r_1^3\right),$$

$$A_3 = \frac{A_4}{\left(1 - \frac{C_2}{r_2^3}\right)}\left[\frac{A_2}{A_4} + \frac{B_2}{A_4}\frac{1}{r_2^3} - \frac{C_1}{r_2^3}\right], \qquad B_3 = A_4\left[C_1 - \frac{A_3}{A_4}C_2\right],$$

$$A_4 = -E_0, \qquad B_4 = A_4 r_3^3\left(\frac{A_3}{A_4} + \frac{B_3}{r_3^3 A_4} - 1\right), \tag{6}$$

and

$$C_1 = \frac{3}{2}\frac{\epsilon_4}{(\epsilon_4 - \epsilon_3)}r_3^3, \qquad C_2 = \frac{1}{2}\frac{(2\epsilon_4 + \epsilon_3)}{(\epsilon_4 - \epsilon_3)}r_3^3, \qquad C_3 = \epsilon_2 - \frac{\left(1 + \frac{2}{r_2^3}C_2\right)}{\left(1 - \frac{C_2}{r_2^3}\right)}\epsilon_3,$$

$$C_4 = 2\epsilon_2 + \frac{\left(1 + \frac{2}{r_2^3}C_2\right)}{\left(1 - \frac{C_2}{r_2^3}\right)}\epsilon_3, \quad C_5 = \epsilon_3\frac{C_1}{r_2^3}\left[2 + \frac{\left(1 + \frac{2}{r_2^3}C_2\right)}{\left(1 - \frac{C_2}{r_2^3}\right)}\right], \tag{7}$$

It is worth noting that (Eq. 7) is used first to obtain the coefficients B_2 and A_2. After that, the remainder coefficients can be determined.

The induced electric field in the host medium outside the shell is given by

$$\boldsymbol{E}_4 = \left[2\left(1 - \frac{A_3}{A_4} - \frac{B_3}{r_3^3 A_4}\right)\left(\frac{r_3^3}{r^3}\right) + 1\right]E_0\cos(\theta)\,\hat{\boldsymbol{r}} + \left[\left(1 - \frac{A_3}{A_4} - \frac{B_3}{r_3^3 A_4}\right)\left(\frac{r_3^3}{r^3}\right) - 1\right]E_0\sin(\theta)\,\widehat{\boldsymbol{\theta}}, \tag{8}$$

which is the same as a dipole field with a dipole moment of $\boldsymbol{p} = \epsilon_4\alpha\boldsymbol{E_0}$ where the polarizability α is given by

$$\alpha = 4\pi\epsilon_0 r_3^3\left(1 - \frac{A_3}{A_4} - \frac{B_3}{r_3^3 A_4}\right). \tag{9}$$

The total loss of illuminating radiation on the nanoparticles is characterized by the extinction cross section which is the sum of scattering and absorption cross sections [58,59]

$$\sigma_{\text{ext}} = \sigma_{\text{sca}} + \sigma_{\text{abs}}, \tag{10-a}$$

$$\sigma_{\text{sca}} = \frac{1}{6\pi\epsilon_0^2} k^4 |\alpha|^2, \qquad \sigma_{\text{abs}} = \frac{k}{\epsilon_0} \text{Im}(\alpha), \tag{10-b}$$

where $k \sim 2\pi\sqrt{\epsilon_4}/\lambda$ in the limit of a low-density nanoparticles.

In this paper, we assume the dielectric constant for the silica core at all wavelengths to be $2.07 + 0j$ [18,60] and the surrounding medium is an aqueous medium with $\epsilon_4 = 1.77 + 0j$ [18,58]. The dielectric function of gold and silver shell (or core) is calculated using the Lorentz-Drude model with considering the size−dependent electron scattering where [58]

$$\epsilon(a,\omega) = \epsilon(\omega)_{\text{exp}} + \frac{\omega_p^2}{\omega^2 + j\omega\Gamma_0} - \frac{\omega_p^2}{\omega^2 + j\omega\Gamma}. \tag{11}$$

In (Eq. 11), $\epsilon(\omega)_{\text{exp}}$ is the experimental bulk dielectric function, ω_p is the bulk plasma frequency, Γ_0 is the bulk collisional frequency. $\Gamma \sim \Gamma_0 + v_f/a$ is the modified bulk collisional frequency where v_f is the Fermi velocity and a is the effective mean free path of electrons (i.e., the shell thickness or the core radius). $\epsilon(\omega)_{\text{exp}}$ is calculated follwing the results reported in [61] where

$$\epsilon(\omega)_{\text{exp}} = 1 - \frac{\Omega_p^2}{\omega^2 + j\omega\Gamma_0} + \sum_{j=1}^{p} \frac{f_j\omega_p^2}{(\omega_j^2 - \omega^2) - j\omega\Gamma_j}. \tag{12}$$

Equation (12) includes the contribution of the intraband and interband effects. $\Omega_p = \sqrt{f_0}\omega_p$ is the plasma frequency associated with intraband transitions with oscillator strength f_0 and damping constant Γ_0. The interband part of the dielectric function is described by the Lorentz model where p is the number of oscillators with frequency ω_j, strength f_j, and lifetime $1/\Gamma_j$. In this study, all parameters shown in (Eqs. 11 and 12) are assumed as reported in [61].

For a graphene layer, the relative dielectric function takes the form of [62]

$$\epsilon(a,\omega) = 5.5 + j\frac{\sigma_{\text{tot}}}{\epsilon_0\omega t_g}, \tag{13}$$

where σ_{tot} is the total optical conductivity taking into account the intraband and interband transitions, and $t_g(in\ nm) = N \times 0.34$ is the thickness of the graphene shell where N is the number of graphene layers. σ_{tot} is given using the Kubo formula as [62,63]

$$\sigma_{\text{tot}} = \sigma_{\text{real}} + j\sigma_{\text{imag}}, \tag{14-a}$$

$$\sigma_{\text{real}} = \frac{\sigma_0 H}{2}\left[\tanh\left(\frac{\hbar\omega + 2\mu}{4k_B T}\right) + \tanh\left(\frac{\hbar\omega - 2\mu}{4k_B T}\right)\right], \tag{14-b}$$

$$\sigma_{\text{imag}} = \frac{4\mu\sigma_0}{\pi\hbar\omega}\left(1 - \frac{2}{9}\left(\frac{\mu}{t}\right)^2\right) - \frac{\sigma_0 H}{\pi}\log\left(\frac{|\hbar\omega + 2\mu|}{|\hbar\omega - 2\mu|}\right), \tag{14-c}$$

where μ is the Fermi energy (chemical potential), $\sigma_0 = e^2/4\hbar$, $H = [1 + (\hbar\omega/6t)^2]$, k_B is Boltzmann's constant, T is the temperature, and t is the hopping parameter. In (Eq. 14), t is taken as 2.7 eV at temperature of 300 K and μ is in the range 0 eV to 1.5 eV.

Results and Discussions

It is worthy to spot first on LSPRs of the nanocomposite without outer shells. Figure 2a and b show the absorption efficiency spectra σ_{abs} for a spherical SiO_2 core wrapped with gold and silver, Gold@SiO_2 and Silver@SiO_2, respectively, at different ratios of the core to shell radius r_1/r_2 where $r_2 = r_1 + d$. Here, the core radius r_1 is kept constant at 30 nm while the shell thickness d is varied. Four pairs of values are considered for these two degrees of freedom, (r_1/r_2, d) = (0.55,24nm), (0.62,18nm), (0.71,12nm) and (0.83,6nm). The shell thicknesses of gold (or silver) are assumed to be larger than that of the graphene shell (~0.34 nm) since it is set to ensure that the plasmon resonance occurs within the valid frequency range of (Eq. 11). Figure 2 indicate the LSPRs of both gold and silver wrapped dielectric cores are in the visible light region. Also, the absorption intensity associated with a red-shift of the LSPR is reduced with decreasing the values of r_1/r_2 and d. That is, the Fig. indicates tuning of the LSPRs wavelength with varying the geometry of the plasmonic metal-dielectric nanocomposite, which agrees with the investigations in [18]. According to the hybridization theory based on the quasi−static approximation [64,65], the shown LSPR peak corresponds to the coupled plasmon (antisymmetric dipole-like) mode which is induced as hybridization of the sphere and cavity modes formed on outer and inner surfaces of the shell, respectively. This type of hybridized mode was analyzed in details in [43] and was shown to exhibit a red shift with the increase of the shell thickness. The Fig. shows also that the absorption of Silver@SiO_2 is almost four times better than that of Gold@SiO_2. Despite these advantages, there is no significant variation in the linewidth of the revealed LSPR peaks.

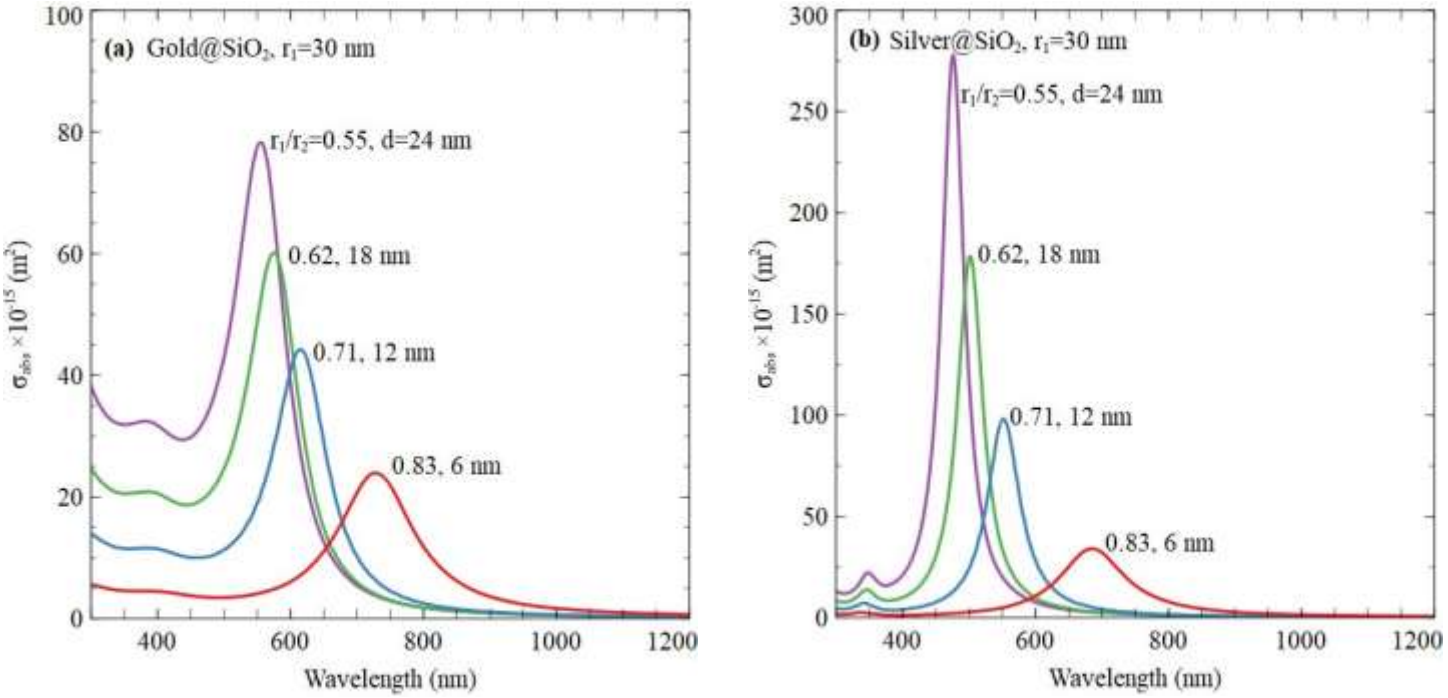

Fig. 2 Wavelength spectra of the absorption cross section σ_{abs} for SiO_2 core wrapped with (a) gold shell (Gold@SiO_2), and (b) silver shell (Silver@SiO_2), at ratios of the core radius r_1/r_2 and shell thickness d of (r_1/r_2, d) = (0.55,24nm), (0.62,18), (0.71,12nm) and (0.83,6nm).

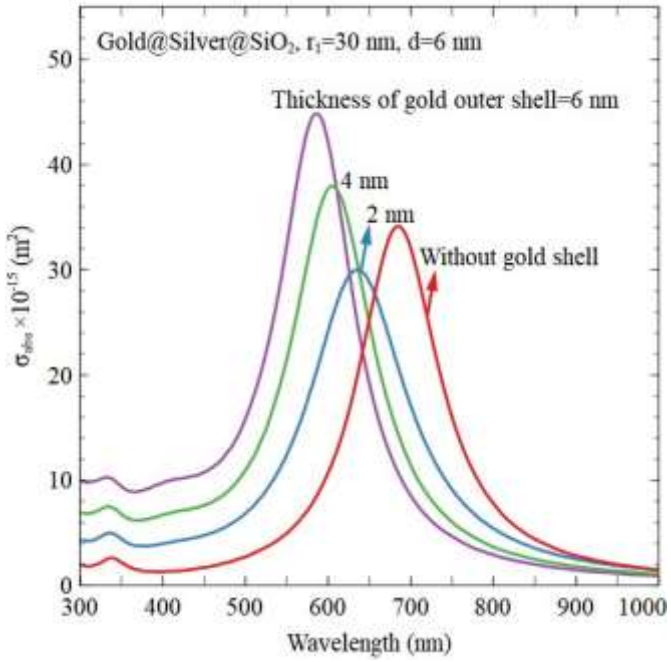

Fig. 3 Wavelength spectra of the absorption cross section σ_{abs} of the SiO_2 core wrapped with silver and then gold shells with gold layer thickness of 2, 4 and 6 nm.

In Fig. 3, we spot on the results of LSPRs of core-bimetallic shells (without a graphene shell). The Fig. plots the spectra of absorption cross section σ_{abs} of wrapping the Silver@SiO_2 nanostructure with a gold shell; that is, absorption efficiency of a dielectric core wrapped with bi-metallic shells. The shown spectra correspond to gold layer thickness of 2, 4 and 6 nm. The Fig. shows a blue-shift of LSPRs of the Gold@Silver@SiO_2 structure. The shifted peak then corresponds to the coupled LSPR mode of both gold and silver. The new peak appears to shift towards shorter wavelengths as the gold-layer thickness increases, which is also associated with an increase in intensity. It is also worth noting that this blue-shift of the LSPRs is not accompanied by any remarkable changes in the linewidth of the absorption peak. Overall, in the absorption spectra of Gold@Silver@SiO_2 and Gold@SiO_2 (or Silver@ SiO_2) nanostructures shown in Figs. 3 and 2, respectively, the LSPRs have a rather wide bandwidth, which is not appropriate for highly sensitive sensing applications.

The significance of using graphene as an outer shell to the dielectric core-gold (or silver) shell nanostructures is demonstrated in Fig. 4. Figure 4a and b plot the wavelength spectra of the absorption coefficient of core-bishell nanoparticles, Graphene@Gold@SiO_2 and Graphene@Silver@SiO_2, respectively, at different values of the chemical potential μ. The Fig. correspond to SiO_2 sphere of radius r_1=30nm, gold and silver thickness d=6nm, and a single layer of graphene with thickness t_g = 0.34 nm. Figure 4a and b show improvements of the absorption coefficient of the Silver@SiO_2 nanostructure due to wrapping by graphene instead of gold (Fig. 3) or without using any outer shell (Fig. 2). In both Figs., when the chemical potential μ is small, we can get two separate peaks, one in the visible region and the second is in the NIR region due to hybridization of LSPRs of the metal-dielectric and graphene shell, respectively [43]. The latter peak in NIR region makes the structure promising for use in medical applications, such as thermal phototherapy [54-57]. This LSRP peak is ultra-narrow and can be tuned in the NIR region by varying μ; the increase of μ from 1.0 to 1.4eV causes blue shifting of the graphene LSPR peak from ~920 nm to 745 nm in Graphene@Gold@SiO_2 of Fig. 4a, while the increase of μ from 1.0 to 1.6eV shifts the peak from ~920 nm to 700 nm in Graphene@Silver@SiO_2 of Fig. 4b. It is interesting to notice that when the graphene-induced peak approaches the LSRP of Gold@SiO_2 or of Silver@SiO_2, these peaks split into two narrow peaks with small linewidths of ~40 nm.

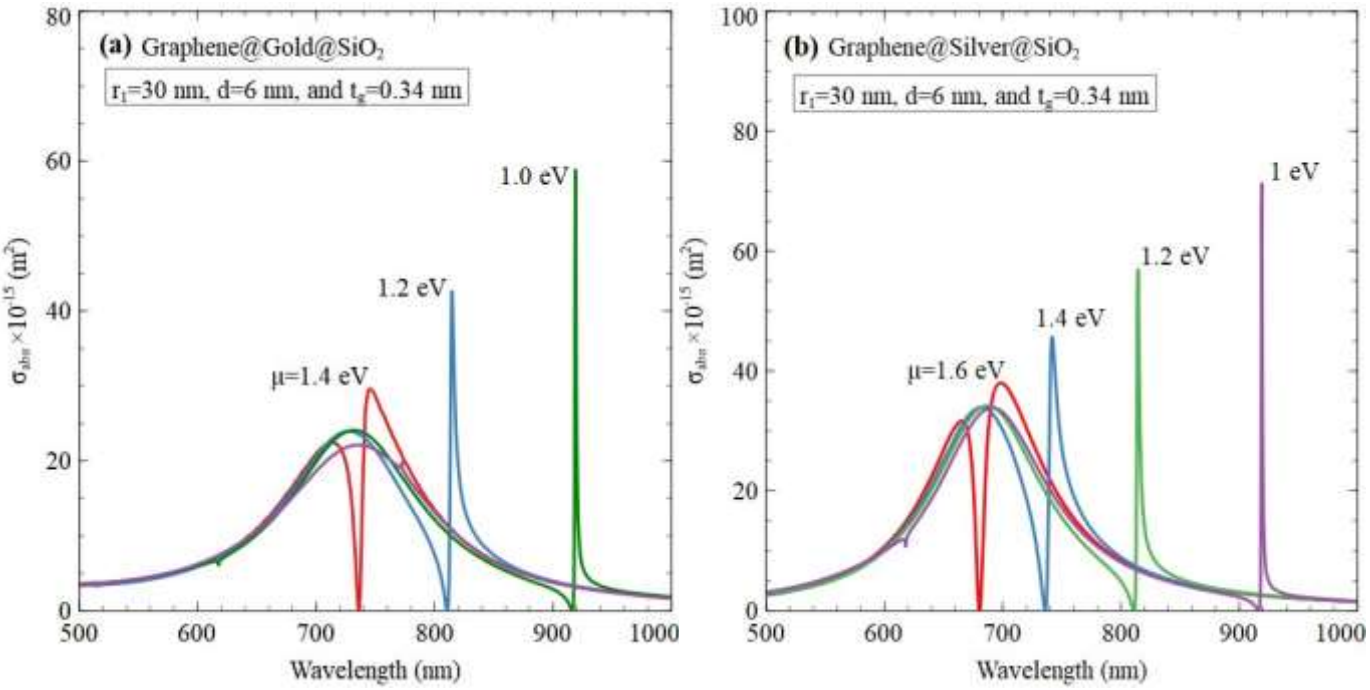

Fig. 4 Wavelength spectra of the absorption coefficient σ_{abs} of (a) Graphene@Gold@SiO_2, and (b) Graphene@Silver@SiO_2 nanostructures at values of chemical potential μ between 1.0 and 1.6eV when r_1=30nm, d=6nm and t_g = 0.34nm.

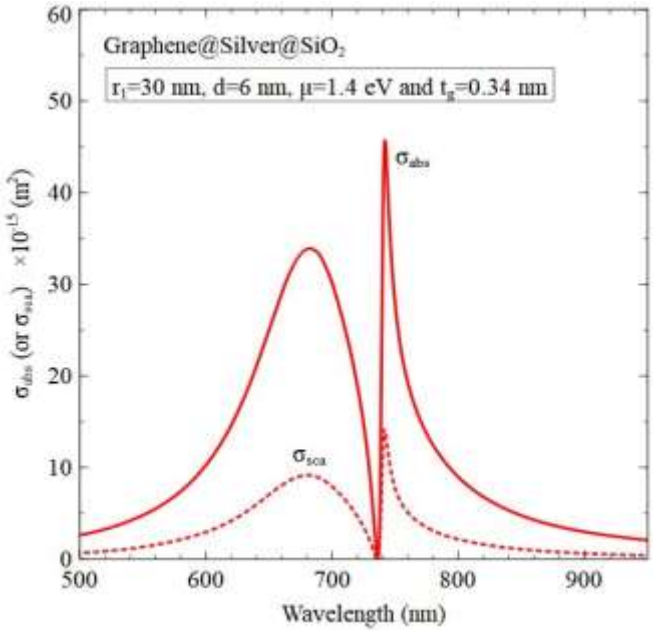

Fig. 5 Comparison between the absorption and scattering spectra of Graphene@Silver@SiO_2 when r_1=30nm, d=6nm, $\mu = 1.4\ eV$, and t_g = 0.34nm.

Another interesting character of the graphene assisted LSPR in the investigated bi-shell nanostructures is illustrated in Fig. 5, which compares the wavelength spectrum of the absorption cross section σ_{abs} with that of the scattering cross section σ_{sca} for Graphen@Silver@SiO_2. The Fig. shows that the spectrum of σ_{abs} is almost 4 times higher than that of σ_{sca}. That is, the total extinction of the graphene-based bishells is mainly due to the absorption process.

In Fig. 6, we demonstrate the influence of increasing the number of graphene layers on the LSPR of the Graphen@Silver@SiO_2 nanostructure. Figure 6 plots the spectrum of σ_{abs} for the number of graphene layers N = 1, 2, 4 and 6 when r_1=30nm, d=6nm, and $\mu = 1.4\ eV$. The Fig. shows a small red shift of the coupled LSPR mode of the silica core with the silver shell (~from 670 to 710nm) with the increase of N. Also, the Fig. shows that the graphene assisted LSRP narrow peak shifts significantly towards longer wavelengths in the NIR region as the number of layers increases. The split peak occurs at λ~750 nm when N=1, while it becomes separated when N≥2. That is, the narrow NIR-peak assisted by graphene can be tuned to the NIR therapeutic window (700-900 nm and 1000-1700 nm) by varying the number of graphene layers.

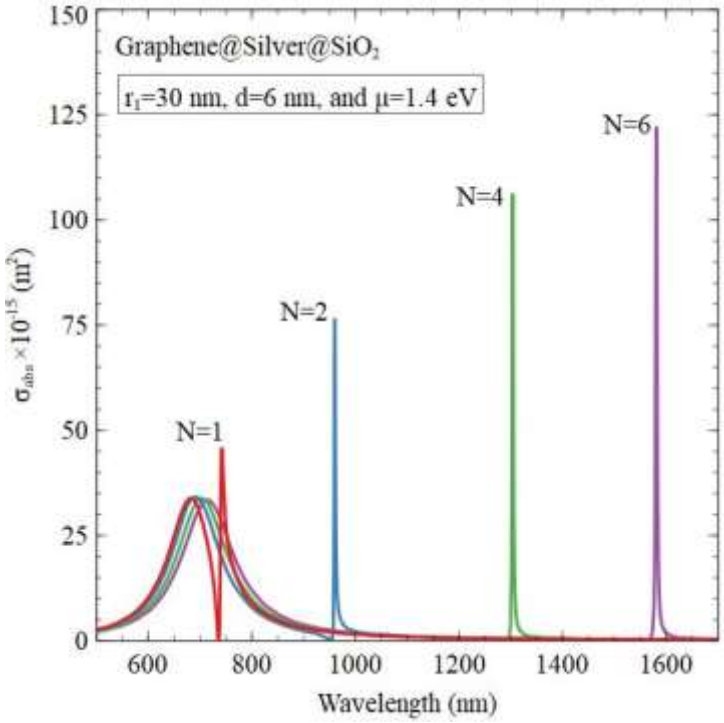

Fig. 6 The absorption cross-section spectra σ_{abs} of Graphene@Silver@SiO_2 at different values of the number of graphene layers N when r_1=30nm, d=6nm, and $\mu = 1.4\ eV$.

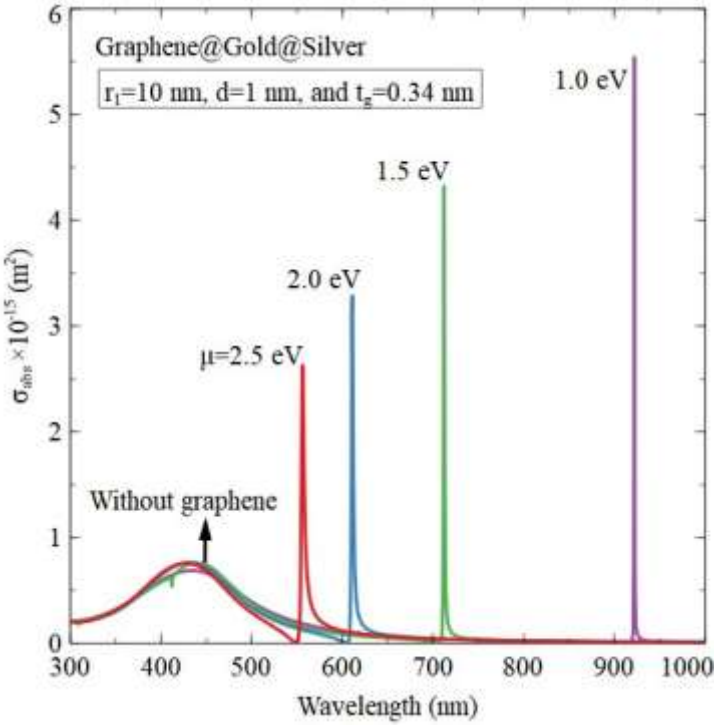

Fig. 7 Wavelength spectra of the absorption coefficient σ_{abs} when the dielectric core is replaced by silver, Graphene@Gold@Silver, at values μ = 1.0, 1.5, 2.0 and 2.5 eV when r_1=10nm, d=1nm, and t_g = 0.34nm.

It is practically important to compare the present results when the dielectric core (Fig. 4a) is replaced by silver as a typical plasmonic material. Figure 7 shows that the coupled LSPR mode of the silver core with gold shell occurs at the wavelength of ~440 nm. Similar to Fig. 4a, Fig. 7 indicates also shift of the LSRP narrow peak of graphene to lower wavelength towards the visible light region with the increase of the chemical potential μ. However, shifting such a narrow peak to the location of the LSRP peak of the Gold@Silver structure and the consequent split of the latter peak into narrower peaks requires impractical chemical potential higher than 2.5 eV.

Conclusion

We exploit the quasi-static formulation to explore the LSPRs of core-bishell nanoparticles composed of a graphene outer shell wrapped around a metallic inner shell surrounding a dielectric core. Two LSPR peaks are exhibited in the absorption spectra of the proposed graphene-assisted core-bishell particles. The first LSPR peak in the visible range corresponds to the coupled plasmon (antisymmetric dipole-like) mode which is induced by the inner metal shell and the dielectric core. The second LSPR peak in the NIF range and corresponds to graphene plasmons

induced at the surface of the graphene outer shell. As it has an ultra-narrow linewidth in the NIR spectral range, the graphene's second LSPR could be valuable for medical applications, for instance in phototherapy. By varying the optical properties of graphene shell, the graphene LSPR can also be adjusted to the position of the first LSPR splitting it into two narrow linewidth peaks in the visible range. The resultant resonance peaks may be advantageous for LSPR-based sensors with high sensitivity. Furthermore, we demonstrate the advantageous of the LSPRs observed in the proposed nanoparticles over those observed in the conventional core (dielectric)-shell (metal) nanoparticles as well as core-bishell nanoparticles when the graphene outer shell is replaced by a different metal shell.

Author Contribution H. Fares: Conceptualization, methodology, data curation, validation, formal analysis, writing - review and editing. **M. Ahmed:** Data curation, validation, formal analysis, writing - original draft preparation, writing - review and editing. **S. Moustafa:** Methodology, data curation, validation, formal analysis, writing - review and editing.

Funding The research reported in this publication was supported by funding from Assiut University and Taibah University.

Declaration of competing interest

The authors declare no competing financial interest.

Data availability

The data that support the findings of this study are available from the corresponding author upon reasonable request.

References

1. Loiseau A, Asila V, Boitel-Aullen G, Lam M, Salmain M, Boujday S (2019) Silver-based plasmonic nanoparticles for and their use in biosensing. Biosensors 9(2):78
2. Tricoli A, Nasiri N, De S (2017) Wearable and miniaturized sensor technologies for personalized and preventive medicine. Adv Funct Mater 27(15):1605271
3. Riboh JC, Haes AJ, McFarland AD, Ranjit C, Van Duyne RPJ (2003) A nanoscale optical biosensor: real-time immunoassay in physiological buffer enabled by improved nanoparticle adhesion. Phys Chem B 107(8):1772-1780
4. Shafer-Peltier KE, Haynes CL, Glucksberg MR, Van Duyne RPJ (2003) Toward a glucose biosensor based on surface-enhanced Raman scattering. J Am Chem Soc 125(2):588-593
5. Grainger RG (1982) Intravascular contrast media—the past, the present and the future. Mackenzie Davidson Memorial Lecture, April 1981. Br J Radiol 55(649):1-18
6. Yelin D, Oron D, Thiberge S, Moses E, Silberberg Y (2003) Multiphoton plasmon-resonance microscopy. Opt Express 11(12):1385-1391
7. Wang Y, Xie X, Wang X, Ku G, Gill KL, O'Neal DP, Stoics G, Wang LV (2004) Photoacoustic tomography of a nanoshell contrast agent in the in vivo rat brain. Nano Lett 4(9):1689-1692
8. El-Sayed IH, Huang X, El-Sayed MA (2005) Surface plasmon resonance scattering and absorption of anti-EGFR antibody conjugated gold nanoparticles in cancer diagnostics:

applications in oral cancer. Nano Lett 5(5):829-834
9. Rosi NL, Mirkin CA (2005) Nanostructures in biodiagnostics. Chem Rev 105(4):1547-1562
10. Chen J, Wiley B J, Li Z Y, Campbell D, Saeki F, Cang H, Leslie A, Lee J, Li X, Xia Y (2005) Gold nanocages: engineering their structure for biomedical applications. Adv Mater 17(18):2255-2261
11. Liu C, Liu Z, Lv J, Sun T, Liu Q, Mu H, Chu PK (2017) Analysis of Local Surface Plasmon Resonance in Multilayered Au/Ag/Graphene Nanoshells. NANO 12(05):1750062
12. Gulati A, Liao H, Hafner JH (2006) Monitoring gold nanorod synthesis by localized surface plasmon resonance. J Phys Chem B 110(45):22323-22327
13. Nehl C, Liao H, Hafner J (2006) Optical properties of star-shaped gold nanoparticles. Nano Lett 6(4):683-688
14. Hao F, Nehl CL, Hafner JH, Nordlander P (2007) Plasmon resonances of a gold nanostar. Nano Lett 7(3):729-732
15. Wang H, Brandl D, Le F, Nordlander P, Halas N (2006) Nanorice: a hybrid plasmonic nanostructure. Nano Lett 6(4):827-832
16. Cang H, Sun T, Li Z, Chen J, Wiley B, Xia Y, Li X (2005) Gold nanocages as contrast agents for spectroscopic optical coherence tomography. Opt Lett 30(22):3048-3050
17. Hu Y, Fleming RC, Drezek RA (2008) Optical properties of gold-silica-gold multilayer nanoshells. Opt Express 16(24):19579-19591
18. Jain PK, El-Sayed MA (2007) Universal scaling of plasmon coupling in metal nanostructures: Extension from particle pairs to nanoshells. Nano Lett 7(9):2854–2858
19. Zhang K, Gao L (2007) Optical bistability in graphene-wrapped dielectric nanowires. Opt Express 25(12):13747-13759
20. Geim AK (2009) Graphene: Status and prospects. Science 324(5934):1530–1534
21. Nair RR, Blake P, Grigorenko AN, Novoselov KS, Booth T J, Stauber T, Peres NM, Geim AK (2008) Fine structure constant defines visual transparency of graphene. Science 320(5881):1308
22. Bonaccorso F, Sun Z, Hasan T, Ferrari AC (2010) Graphene photonics and optoelectronics. Nat photonics 4(9):611-22
23. Mueller T, Xia F, Avouris P (2010) Graphene photodetectors for high-speed optical communications. Nat photonics 4(5):297-301
24. Cai X, Sushkov AB, Jadidi MM, Nyakiti LO, Myers-Ward RL, Gaskill DK, Murphy TE, Fuhrer MS, Drew HD (2015) Plasmon-enhanced terahertz photodetection in graphene. Nano Lett 15(7):4295-4302
25. Lee SH, Choi M, Kim TT, Lee S, Liu M, Yin X, Choi HK, Lee SS, Choi CG, Choi SY, Zhang X (2012) Switching terahertz waves with gate-controlled active graphene metamaterials. Nat Mater 11(11):936-941
26. Wan M, Li Y, Chen J, Wu W, Chen Z, Wang Z, Wang H (2017) Strong tunable absorption enhancement in graphene using dielectric-metal core-shell resonators. Sci Rep 7(1):32-41
27. Wang X, Zhi L, Müllen K (2008) Transparent, conductive graphene electrodes for dye-sensitized solar cells. Nano Lett 8(1): 323–327
28. Mak KF, Sfeir MY, Wu Y, Lui CH, Misewich JA, Heinz TF (2008) Measurement of the optical conductivity of graphene. Phys Rev Lett 101(19): 196405-196408
29. Shi Z, Yang Y, Gan L, Li ZY (2016) Broadband tunability of surface plasmon resonance in graphene-coating silica nanoparticles. Chin Phys B 25(5):057803-057809
30. Yang B, Wu T, Yang Y, Zhang X (2015) Tunable subwavelength strong absorption by graphene wrapped dielectric particles. J Opt 17(3):035002-035007
31. Singh A, Shishodia MS (2020) Graphene vs. silica coated refractory nitrides based core-shell nanoparticles for nanoplasmonic sensing. Physica E 124:114288-114294
32. Schuller JA, Barnard ES, Cai W, Jun YC, White JS, Brongersma ML (2010) Plasmonics for extreme light concentration and manipulation. Nat Mater 9(3):193-204.
33. Echtermeyer TJ, Britnell L, Jasnos PK, Lombardo A, Gorbachev RV, Grigorenko AN, Geim

AK, Ferrari AC, Novoselov KS (2011) Strong plasmonic enhancement of photovoltage in graphene. Nat Commun 2(1): 458-462
34. Liu Y, Cheng R, Liao L, Zhou H, Bai J, Liu G, Liu L, Huang Y, Duan X (2011) Plasmon resonance enhanced multicolour photodetection by graphene. Nat Commun 2(1): 579-585
35. Fang Z, Liu Z, Wang Y, Ajayan PM, Nordlander P, Halas NJ (2012) Graphene-antenna sandwich photodetector. Nano Lett 12(7):3808-3813
36. Hashemi M, Farzad MH, Mortensen NA, Xiao S (2013) Enhanced absorption of graphene in the visible region by use of plasmonic nanostructures. J Opt 15(5):055003-055007
37. Zhu X, Shi L, Schmidt MS, Boisen A, Hansen O, Zi J, Xiao S, Mortensen NA (2013) Enhanced light–matter interactions in graphene-covered gold nanovoid arrays. Nano Lett 13(10):4690-4696
38. Zhao B, Zhao JM, Zhang ZM (2014) Enhancement of near-infrared absorption in graphene with metal gratings. Appl Phys Lett 105(3):031905 -031908
39. Lu H, Cumming BP, Gu M (2015) Highly efficient plasmonic enhancement of graphene absorption at telecommunication wavelengths. Opt Lett 40(15):3647-3650
40. Cai Y, Zhu J, Liu QH (2015) Tunable enhanced optical absorption of graphene using plasmonic perfect absorbers. Appl Phys Lett 106(4):043105 -043108
41. Xiong F, Zhang J, Zhu Z, Yuan X, Qin S (2015) Ultrabroadband, more than one order absorption enhancement in graphene with plasmonic light trapping. Sci Rep 5(1):16998-16705
42. Li Y, He X, Wan M, Wu W, Chen Z (2016) Unconventional Fano effect based spectrally selective absorption enhancement in graphene using plasmonic core-shell nanostructures. Appl Phys Lett 109(3):031909-031913
43. Fares H, Almokhtar M, Almarashi J Q M, Rashad M, Moustafa S (2022) Tunable narrow-linewidth surface plasmon resonances of graphene-wrapped dielectric nanoparticles in the visible and near-infrared. Phys. E: Low-Dimens. Syst. Nanostructures, 115300, IN PRESS
DOI: https://doi.org/10.1016/j.physe.2022.115300
44. Herrera LJ, Scaffardi LB, Schinca DC (2016) High spectral field enhancement and tunability in core–double shell metal–dielectric–metal spherical nanoparticles. RSC Adv 6(112):110471-110481
45. Knauer A, Thetea A, Li S, Romanus H, Csáki A, Fritzsche W, Köhler JM (2011) Au/Ag/Au double shell nanoparticles with narrow size distribution obtained by continuous micro segmented flow synthesis. Chem Eng J 166:1164–1169
46. Tarparelli R, Iovine R, La Spada L, Vegni L (2014) Surface plasmon resonance of nanoshell particles with PMMA-graphene core. COMPEL - Int J Comput Math Electr Electron Eng 33:2016-2029
47. Hu Y, Fleming RC, Drezek RA (2008) Optical properties of gold-silica-gold multilayer nanoshells. Opt Express 16(24):19579-19591
48. Daneshvar e Asl S, Sadrnezhaad SK (2020) Gold@ Silver@ Gold Core Double-Shell Nanoparticles: Synthesis and Aggregation-Enhanced Two-Photon Photoluminescence Evaluation. Plasmonics 15(2):409-416
49. Kale PG, Sahoo MK, Sadual NK, Behera SK (2018) Synthesis of Graphene-wrapped Silicon Nanoparticles by Ultra-sonication. IOP Conf Ser: Mater Sci Eng 338(1):012034-012038
50. Vasilopoulos V, Pitou M, Fekas I, Papi R, Ouranidis A, Pavlidou E, Patsalas P, Choli-Papadopoulou T (2020) Graphene-wrapped copper nanoparticles: an antimicrobial and biocompatible nanomaterial with valuable properties for medical uses. ACS omega 5(41):26329-26334
51. Qin Y, Yuan J, Zhang L, Zhao B, Liu Y, Kong Y, Cao J, Chu F, Tao Y, Liu M (2015) Rationally Designed 3D Fe and N Codoped Graphene with Superior Electrocatalytic Activity toward Oxygen Reduction. Small 11:2549–2553
52. Shankar P, Ishak MH, Padarti JK, Mintcheva N, Iwamori S, Gurbatov SO, Lee JH, Kulinich SA (2020) ZnO@ graphene oxide core@ shell nanoparticles prepared via one-pot approach based on laser ablation in water. Appl Surf Sci 531:147365

53. Zhou KY, Chen GY, Liu JA, Zhang ZP, Sun P, Zhang WZ, Niu F, Zhang WX, Liang JC (2016) Cobalt nanoparticles encapsulated in N-doped graphene nanoshells as an efficient cathode electrocatalyst for a mechanical rechargeable zinc–air battery. RSC Adv 6(93):90069-90075
54. Wang X, Wang X, Cheng S, Ye M, Zhang C, Xian Y (2020) Near-infrared light-switched MoS2 nanoflakes@ gelatin bioplatform for capture, detection, and nondestructive release of circulating tumor cells. Anal Chem 92(4):3111-3117
55. Carrasco E, Del Rosal B, Sanz- Rodríguez F, De La Fuente AJ, Gonzalez PH, Rocha U, Kumar KU, Jacinto C, Solé JG, Jaque D (2015) Intratumoral thermal reading during photo-thermal therapy by multifunctional fluorescent nanoparticles. Adv Funct Mater 25(4):615-626
56. Gobin AM, Lee MH, Halas NJ, James WD, Drezek RA, West JL (2007) Near-infrared resonant nanoshells for combined optical imaging and photothermal cancer therapy. Nano Lett 7(7):1929-1934
57. Chen YW, Chen PJ, Hu SH, Chen IW, Chen SY (2014) NIR- triggered synergic photo-chemothermal therapy delivered by reduced graphene oxide/carbon/mesoporous silica nanocookies. Adv Funct mater 24(4):451-459
58. Averitt RD, Westcott SL, Halas NJ (1999) Linear optical properties of gold nanoshells. JOSA B 16(10):1824-1832
59. Neeves AE, Birnboim MH (1989) Composite structures for the enhancement of nonlinear-optical susceptibility. JOSA B 6(4):787-796
60. Malitson IH (1965) Interspecimen comparison of the refractive index of fused silica. J Opt Soc Am 55(10):1205-1209
61. Rakić AD, Djurišić AB, Elazar JM, Majewski ML (1998) Optical properties of metallic films for vertical-cavity optoelectronic devices. Appl Opt 37(22):5271-5283
62. Matthaiakakis N, Mizuta H, Charlton MD (2016) Strong modulation of plasmons in Graphene with the use of an Inverted pyramid array diffraction grating. Sci Rep 6(1):27550
63. Kravets VG, Grigorenko AN, Nair RR, Blake P, Anissimova S, Novoselov KS, Geim AK (2010) Spectroscopic ellipsometry of graphene and an exciton-shifted van Hove peak in absorption. Phys Rev B 81(15):155413- 155418
64. Prodan E, Radloff C, Halas NJ, Nordlander P (2003) A hybridization model for the plasmon response of complex nanostructures. science 302(5644):419-422
65. Prodan E, Nordlander PJ (2004) Plasmon hybridization in spherical nanoparticles. J Chem phys 120(11):5444-5454

Supplementary Files

This is a list of supplementary files associated with this preprint. Click to download.

- SupplementaryMaterial.docx